

Random number generation from a quantum tunneling diode

Kanin Aungskunsiri^{*,†}, Ratthasart Amarit[†], Kruawan Wongpanya, Sakdinan Jantarachote, Wittawat Yamwong, Siriporn Saiburee, Sataporn Chanhorm, Apichart Intarapanich, and Sarun Sumriddetchkajorn

*National Electronics and Computer Technology Center,
National Science and Technology Development Agency,
Ministry of Higher Education, Science, Research, and Innovation,
112 Thailand Science Park, Phahonyothin Road, Khlong Nueng, Khlong Luang, Pathum Thani, 12120 THAILAND*

(Dated: 31 January 2023, [arXiv:2002.02032](https://arxiv.org/abs/2002.02032))

*The author to whom correspondence may be addressed: kanin.aungskunsiri@nectec.or.th.

†These two authors contributed equally to this work.

ABSTRACT

Random numbers are important in many activities, including communication, encryption, science, gambling, finance, and decision-making. There is a strong demand for a hardware random number generator that could support cryptographic applications. In this work, we propose a quantum tunneling diode as a source of true randomness achieved by applying electrical current sweeps through the device and then harnessing a time-counting unit to measure fluctuation of current flows. Our approach can be implemented with inexpensive electronics and could be integrated into systems that require random numbers such as portable communication devices.

Note: *This article may be downloaded for personal use only. Any other use requires prior permission of the author and AIP Publishing. This article appeared in *Appl. Phys. Lett.* **119**, 074002 (2021) and may be found at <https://doi.org/10.1063/5.0055955>.*

Random numbers have many uses in communication, science, mathematics¹, testing, finance, and gambling. In communication, random numbers are critical for the encryption of sensitive information. The security of communication, in a practical sense, relies on the complexity of an encryption function; achieving that complexity, in turn, demands unpredictability of secret keys. In addition to quantum communication, real-world implementation of quantum-key-distribution protocol²⁻⁷ demands true randomness in the process of establishing secret keys between trusted nodes—namely, both the sender and the receiver must randomly select quantum states for transmission and detection respectively. In stochastic simulation, random seeds are used in a mechanism to produce parameter values for simulation models with a variety of probability distributions⁸. Randomization is also key in gambling⁹ and digital lotteries, especially in casinos, where a dedicated random number generator is vital. In the stock market, randomness is involved in a process of stocks distribution to buyers. Furthermore, verification via online transaction requires unpredictably random seeds for the generation of one-time passwords.

Random numbers can be obtained from various processes such as mechanical processes, computer programing¹⁰, chaotic process¹¹⁻¹⁵, radioactive decay¹⁶, atmospheric noise¹⁷, electronic noise¹⁸, and quantum phenomena. However, random number generation via mechanical processes and devices (e.g., coin flipping, Galton boards¹⁹, and lottery wheels) have some intrinsic biases such that outputs are not equally distributed, which results in unreliable randomization.

Computer programing generates pseudo-random numbers at a very fast speed in practice, but this source poses a security issue since an output value is calculated from a deterministic process. Electronic noise appears as a random disturbance in an electrical signal. It can serve a useful purpose for random number generation, but this source consists of intrinsic biases given that it is difficult to derive raw random outputs with good statistical properties. Atmospheric noise relates to a chaotic process that involves complexities cooperating with unknown parameters. Though atmospheric noise may be adequate in some applications, it can pose security risks. Namely, since the random signals are not isolated in a closed system, a third party could set up a device to obtain signals coming from the same origin. Exploitations of a quantum property of light²⁰ in various schemes, such as optical shot noise²¹⁻²³, phase fluctuation of a laser^{24,25}, vacuum fluctuation^{26,27}, and photon arrival time measurements^{28,29}, are approaches to obtain high bitrate quantum random number generation.

Regarding current technologies mentioned above, entropy sources acquired from the quantum origins are still expensive. Other entropy sources relate to the quantum tunneling effect in various semi-conductor devices such as resonant tunneling diodes³⁰, tunnel field-effect transistors³¹, and magnetic tunnel junctions³²⁻³⁵. Among this device category, the tunnel diode as well as its exploitation for high quality random number generation would be of interest.

In this work, we propose an application of a tunnel diode³⁶ as a key component for obtaining an entropy source^{37,38}. This device operates at room temperature and does not require ex-

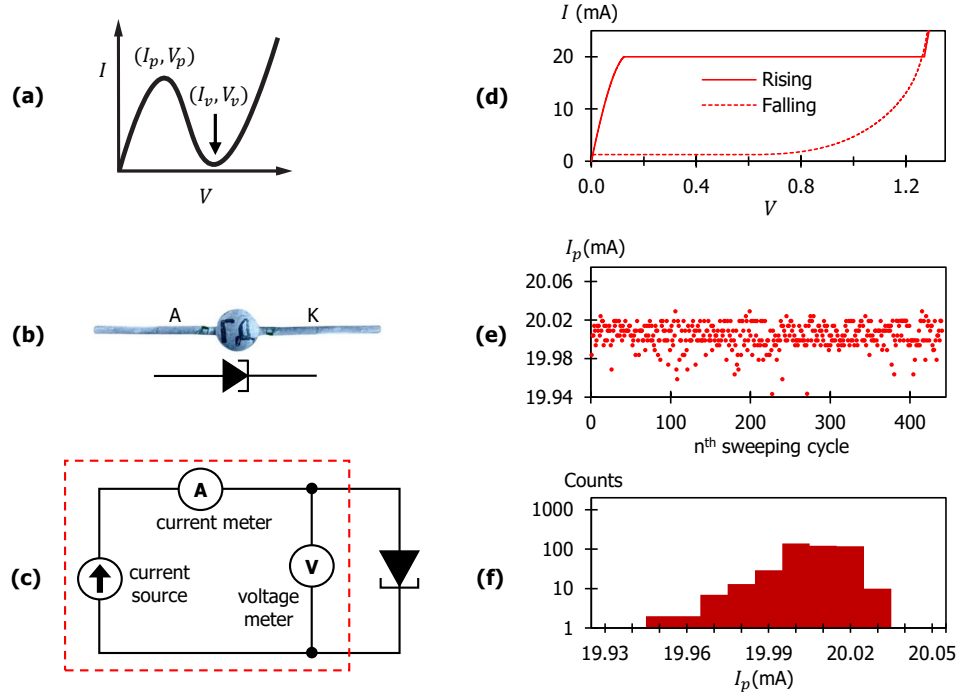


FIG. 1. **(a)** Ideal I-V characteristic of a tunnel diode. **(b)** Tunnel diode used in this work (P/N: 3I201D). **(c)** Circuit diagram of the experiments. **(d)** I-V hysteresis loop measured from single current sweeping (round trip) according to (c). **(e, f)** Experimental results from 450 current sweeps showing (e) extracted values of I_p and (f) distribution of I_p . In (c), equipment within the enclosed dashed line can be replaced with a current-source meter. In (d, e, f), the datasets were taken using a dedicated current-source meter (model: Keithley-2450).

pensive or complicated systems for its practical implementation.

A tunnel diode³⁶ is a solid-state device and one of many types of semi-conductor diodes incorporated with a p-n junction. See the supplementary material for a basic introduction of a tunnel diode. The device itself can operate in two modes: (i) a tunneling mode and (ii) a typical p-n junction mode. An ideal plot of current as a function of biased voltage (I-V characteristic) of a tunnel diode is illustrated in Figure 1a. As the figure shows, a tunnel diode has an N-shaped I-V characteristic such that there is a peak current (I_p) at a specific bias voltage (V_p). This characteristic is due to the collective behavior of tunneling electrons that results in the current flow. In fact, this behavior is different from the case of a single particle described by the quantum mechanics.

Regarding the N-shape of the I-V characteristic, sweeping current (I) and measuring voltage (V) across a tunnel diode results in a hysteresis cycle. We examined an off-the-shelf tunnel diode (P/N: 3I201D), as shown in Figure 1b, with a circuit diagram, as shown in Figure 1c. An I-V hysteresis loop obtained from our measurements is presented in Figure 1d. Here, I_p is associated with the value of current where the voltage jumps to the other branch of the hysteresis loop.

Bernardo-Gavito et al.³⁰ conducted a study of the hysteresis behavior associated with the generation of random numbers, examining the I-V characteristic by performing multiple current sweeps on a resonant-tunneling diode (RTD). In the prior-art, each forward current sweeping through the RTD

took a different path along the I-V curve in a random manner. The values of I_p as measured in their work fluctuated with a random distribution. We adopted this finding and looked for this behavior on a tunnel diode.

We applied a current-source meter to sweep current through a tunnel diode circuit and collected a dataset of I-V values from 450 current sweeps. The extracted values of I_p are presented in Figure 1e and Figure 1f. Here, we obtained fluctu-

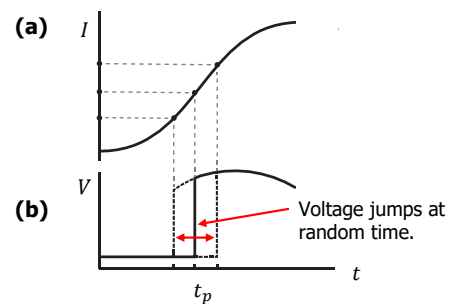


FIG. 2. Method for measuring the value of I_p . A non-negatively sinusoidal waveform, having an amplitude far above the mean value of I_p , is applied for current sweeping through a tunnel-diode circuit. Time-series plots of applied current, as in (a), and measured voltage across a tunnel diode, as in (b), are illustrated together. Here, only the first part of the time-series plots is considered. At $t = t_p$, voltage jumps instantly corresponding to the time that the sweeping current reaches I_p .

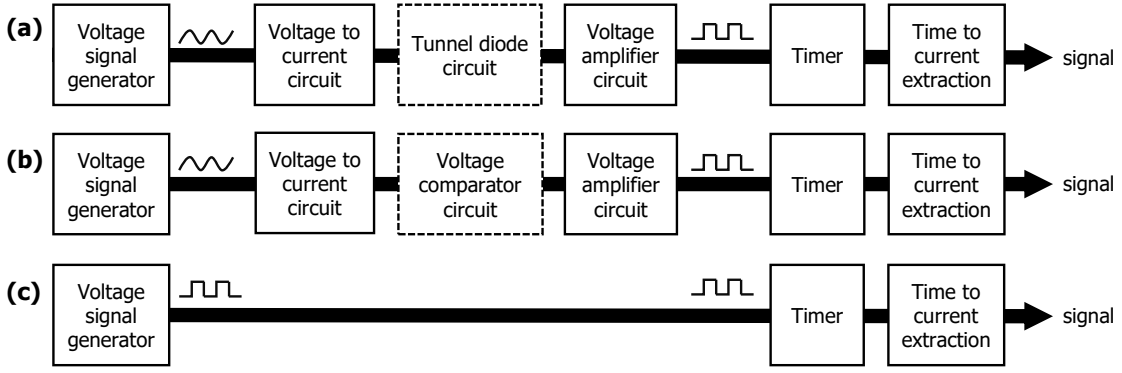


FIG. 3. Flow diagrams of the experiment. We applied a voltage waveform to the electronic circuit and measured the response time for different scenarios: (a) with a tunnel diode circuit, and (b, c) without a tunnel diode circuit. In the beginning, a waveform generator (model: Hantek HDG2022B) was configured to produce non-negatively sinusoidal (a and b) and square (c) voltage with 100 Hz repetition rate. At the end of the flow diagrams, response time was converted to current. In (a), the voltage source was converted to the current source for sweeping the current in non-negatively sinusoidal waveform across the tunnel diode. A timer was implemented to obtain the values of t_p , which subsequently were converted to the values of I_p . In (b, c), the tunnel diode was removed from the circuit to check if any bias signals were originating from other circuit components apart from the tunnel diode itself.

ation of the values of I_p , which behaves in the same manner as found on the RTD³⁰. This outcome suggests the feasibility of harnessing a tunnel diode for random number generation. Unfortunately, a current-source meter is expensive. In addition, datasets acquired from the equipment are discrete-time signals. Detecting the values of I_p that vary in the scale of microampere would be a highly time-consuming form of data acquisition.

Bernardo-Gavito et al.³⁰ demonstrated another method to generate random numbers from the RTD that could be applied with the tunnel diode. Namely, a pulse train of current with constant amplitude was applied for current sweeping. By implementing a proper amplitude, the system generates uniform probability distribution of binary outputs. To sustain uniformity of the outputs, this approach would require a feedback control for real-time adjustment of the pulse-train amplitude.

Alternatively, we propose a simpler method that does not require a feedback control or any complicated system. The values of I_p can be measured by monitoring the change of voltage. In detail, non-negatively sinusoidal waves described as a function of time with an amplitude A and a frequency ω , $I = A \sin(\omega t) + A$, are applied for current sweeping. We set the waveform's amplitude beyond all possible values of I_p as illustrated in Figure 2, so we can be confident that the voltage always jumps to the other branch of the hysteresis loop in every sweeping cycle. Therefore, we can obtain the values of I_p by measuring the values of the current signals at the time a sudden jump of the voltage occurs. As shown in Figure 2, we set $t = 0$ at the beginning of each current sweep. At $t = t_p$, the voltage jumps suddenly. Here, the measured values of t_p are associated with the values of I_p .

Regarding current technologies, we utilized a commercial time-counting unit as a solution for measuring t_p . Namely, a TEENSY® Development Board 4.0, having a retail price of \$19.95, is the generic time-counting module that we implemented in our prototype. This module has a time-resolution

of about 6.7 ns (corresponding to 150 MHz of the sampling rate). The implementation of our method is shown in a flow diagram in Figure 3a. Obtaining the values of t_p allows the values of I_p to be realized by substituting the values of t_p into the relationship $I_p = A \sin(\omega t_p) + A$, as described above.

Two additional measurements were designed to check whether noise was originating from other components. Firstly, we replaced the tunnel diode circuit from the system with a voltage comparator circuit, as shown in Figure 3b, to examine how much the tunnel diode contributed to the fluctuation. Secondly, we checked for bias signals that could come from the

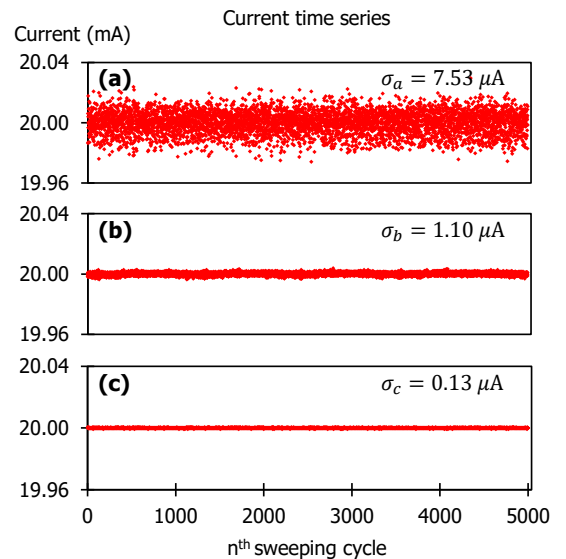


FIG. 4. Current time series obtained from (a) a complete circuit having a tunnel diode circuit, (b) a voltage comparator circuit, and (c) a voltage signal generator, according to circuit diagrams (a)–(c) in Figure 3, respectively.

voltage signal generator by implementing the circuit diagram as depicted in Figure 3c. Data were collected from 5,000 current sweeps for each test. The results are presented in Figure 4.

Figure 4 presents experimental data on the amplitude fluctuation of the current signals measured from three different tests. We calculated the standard deviations (σ) of the datasets and realized that $\sigma_a > \sigma_b > \sigma_c$. Even though we detected noise from other parts of the circuit, the noise is very limited and could be neglectable. The noise might be coming from errors of the experiment; we leave this potential issue for further investigation.

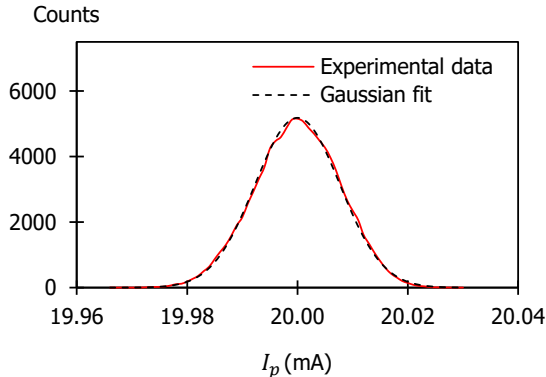


FIG. 5. Histogram showing values of I_p obtained from the tunnel-diode circuit (red solid line) in comparison with a Gaussian model plot (dashed line) featuring the standard deviation of $7.7 \mu\text{A}$. The dataset is collected from 100,000 current sweeps.

By following the flow diagram in Figure 3a, we collected an additional dataset from 100,000 current sweeps and obtained the statistical distribution shown in Figure 5. We incorporated this result that suggests a Gaussian model for determining a suitable amplitude used for the current sweeping. The amplitude which is not too large allows us to obtain signals with good resolution. Accordingly, we managed to collect 20,000 samples per second.

In the implementation, raw signals were collected from the values of t_p . An offset is removed from the raw signals for digitization; consequently, binary outputs, as raw data, were extracted from the entropy source. Next, we followed the NIST SP800-90B³⁹ and implemented a software⁴⁰ provided by the NIST to assess the entropy source. This toolkit consists of two main steps: (i) determining the evaluation track, IID (independent and identically distributed) or non-IID, and (ii) estimating the minimum entropy rate of the raw data depending on the determined track. If the raw data fall into an IID track, entropy is considered from the most common value (MCV) estimation. Otherwise, entropy is assessed from the lowest value of entropy evaluated from 10 estimators, which are (1) MCV estimation, (2) collision estimation, (3) Markov estimation, (4) compression estimation, (5) t-Tuple estimation, (6) longest repeated substring (LRS) estimation, (7) multi most common in window prediction (multiMCW) estimation, (8) lag prediction estimation, (9) multiMMC Prediction estima-

tion, and (10) LZ78Y prediction estimation.

According to the NIST SP800-90B³⁹, our raw data are determined as non-IID. Table I shows the results of min-entropy evaluated from 10 estimators. Five datasets of 40 million-bit sequences were examined. Here, the compression estimation provides the lowest value of min-entropy, given that the assessed min-entropy, H_∞ , was 0.62 on average. This value reflects the lower bound of random bits we can achieve from the raw data. As shown in Table I, the raw data have stable entropy.

These raw data were not ready for real-world use, and they did not pass the NIST SP800-22⁴¹ examination for statistical randomness. Post processing was mandatory to improve the raw data quality. We implemented Toeplitz-hashing extractor^{42,43} with the raw data to render uniformly distributed random outputs. This extractor employs a binary matrix with a dimension of $m \times n$, where m and n correspond to the output and input bit-string length, respectively. m is considered from the value of assessed min-entropy such that $m \leq nH_\infty$. Security parameter is a measure of the statical distance between the distribution of the dataset and the ideal uniform distribution. By implementing the Toeplitz extractor, the security parameter^{42,43} of the post-processed data is estimated from $2^{(m-nH_\infty)/2}$.

In the implementation, we set $n = 4096$. Hence, $m \leq 2539$. We chose $m = 2296$. Thus the Toeplitz matrix has a size of 2296×4096 , providing that the security parameter is below 2^{-100} .

The post-processed data, as the final outputs, were rechecked with the NIST SP800-90B³⁹. The outputs at this stage passed the IID test. Therefore, the min-entropy was determined from the MCV estimation. Table II shows min-entropy assessed from the raw data and the final outputs. The result shows improvement of the statistical properties, and almost full entropy is achieved.

To validate the statistical randomness of the final outputs, a hundred datasets of 1,000,000-bit sequences were examined with 15 sub-methods in accordance to the NIST SP800-22 Test Suite Compliance⁴¹. The test results, as presented in Table III, indicate that the final outputs passed the NIST SP800-22 with a significance level of 0.01.

We also used the same dataset to check for the presence of repeating pattern and evaluate the degree of similarity by performing autocorrelation analysis. As plotted in Figure 6, the result indicates no sign of periodic pattern over 100 successive bit intervals. Therefore, the final outputs have no repeating pattern over an acceptable range.

To conclude, we investigated the I-V characteristic of a tunnel diode and examined the behavior of its hysteresis cycle. Forward current sweeping takes a slightly different path in each cycle. This random variation is associated with the measured values of I_p , and it can serve as an entropy source. We demonstrated a utilization of a time-counting module to measure the values of t_p that are associated with events in which voltages jump to the other branch of the hysteresis loop. As a result, a random distribution was obtained. We demonstrated this proposed technique with inexpensive electronics. Our preliminary prototype used a computer to assess

TABLE I. Entropy assessment of raw data according to the NIST SP800-90B. Each dataset contains 40 million-bit sequences. The values of assessed min-entropy were selected from the lowest values from 10 estimators.

Estimator	Min-entropy				
	Dataset 1	Dataset 2	Dataset 3	Dataset 4	Dataset 5
1. MCV	0.999 313	0.999 373	0.999 259	0.999 325	0.999 403
2. Collision	1.000 000	1.000 000	1.00 0000	1.000 000	1.000 000
3. Markov	0.901 064	0.899 539	0.899 158	0.898 290	0.895 731
4. Compression	0.619 087	0.622 348	0.623 679	0.624 235	0.625 367
5. t-Tuple	0.872 663	0.867 644	0.874 429	0.867 644	0.872 663
6. LRS	0.895 813	0.914673	0.852 600	0.881 406	0.865 663
7. MultiMCW	1.000 000	1.000 000	1.000 000	1.000 000	1.000 000
8. Lag Prediction	0.977 310	0.878 794	0.964 168	0.975 876	0.976 249
9. MultiMMC Prediction	0.853 159	0.855 779	0.857 333	0.855 688	0.855 221
10. LZ78Y Prediction	0.899 739	0.898 203	0.897 819	0.896 944	0.894 367
Assessed min-entropy	0.619 087	0.622 348	0.623 679	0.624 235	0.625 367

TABLE II. Entropy assessment of raw data versus final outputs according to the NIST SP800-90B. Final outputs in each dataset were extracted from 40 million-bit sequences of raw data.

	Assessed min-entropy				
	Dataset 1	Dataset 2	Dataset 3	Dataset 4	Dataset 5
Raw data	0.619 087	0.622 348	0.623 679	0.624 235	0.625 367
Final outputs	0.998 865	0.998 956	0.998 919	0.998 804	0.999 194

TABLE III. NIST SP800-22 test results of 100 million-bit sequences collected from the final outputs. To pass this test suite at a significance level of 0.01, two conditions are required for each of the 15 sub-methods: (i) the P-values-total must be higher than 10^{-4} , and (ii) the proportion must be higher than 96/100.

Method	P-values-total	Proportion	Result
1. Frequency	0.224 821	100/100	Pass
2. Block Frequency	0.779 188	99/100	Pass
3. Runs	0.096 578	99/100	Pass
4. Longest Run	0.304 126	100/100	Pass
5. Rank	0.574 903	99/100	Pass
6. Fast Fourier Transform	0.366 918	98/100	Pass
7. Overlapping Template	0.003 201	99/100	Pass
8. Universal	0.911 413	100/100	Pass
9. Linear Complexity	0.015 598	100/100	Pass
10. Approximate Entropy	0.455 937	99/100	Pass
11. Non-overlapping Template	0.514 124	100/100	Pass
12. Serial	0.249 284	99/100	Pass
13. Cumulative Sums	0.181 557	100/100	Pass
14. Random Excursions	0.062 821	99/100	Pass
15. Random Excursions Variant	0.008 266	99/100	Pass

the entropy rate and process the bit-extraction. By harnessing a time-counting module that allowed us to collect signals at a rate of 20 kHz, we generated random bits, featuring stable and almost full entropy rate, at a speed of 90 kbit/s. The final outputs passed the NIST SP800-22⁴¹, and autocorrelation was not detected.

To construct a random number generator with provable robustness against a security attack, implementation of health-monitoring methodologies in accordance to the NIST SP800-90B³⁹ or AIS 20/31⁴⁴ standard is mandatory. A proper

Autocorrelation

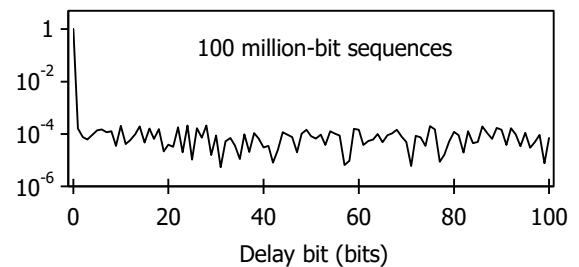


FIG. 6. Autocorrelation calculated from a dataset of 100 million-bit sequences collected from the final outputs.

engineering⁴⁵ to detect failure of the hardware to meet industrial certification would be required before real-world use. The work currently in progress includes improvement of the electronic circuit to eliminate environment bias as well as incorporation of a suitable micro-controller or field programmable gate array (FPGA) to optimize the process of data acquisition and post-processing. This development promises the capability to generate random bits, possibly up to 10 Mbit/s.

ACKNOWLEDGEMENTS

This work was supported by a research program from Thailand's National Electronics and Computer Technology Center, the National Science and Technology Development Agency (NECTEC-NSTDA).

SUPPLEMENTARY MATERIAL

A tunnel diode is a solid-state device and one of many types of semi-conductor diodes incorporated with a p-n junction. In a device, the p-type and n-type are heavily doped. Thus, the tunnel diode is unique in that it exhibits an extremely thin depletion region. Zener diode is another p-n junction diode

that is also heavily doped, but Zener diode is incomparable to the tunnel diode as the former has a relatively lower doping concentration.

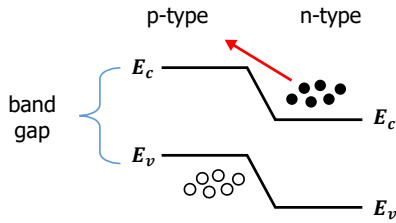


FIG. S1. Energy level of a p-n semiconductor. The band gap between the conduction band (E_c) and the valence band (E_v) of a typical p-n junction diode is wide and behaves like a thick barrier. This barrier blocks the passage of electrons flowing across the p-n junction. Electrons with energy greater than the barrier can overcome the internal potential force and cause a current flow.

In the case of a typical p-n junction diode, the n-type conduction band aligns at the p-type bandgap (Figure S1). In this scenario, the depletion region behaves like a potential barrier that blocks the passage of electrons flowing from p-type to n-type. The current can flow only when the electrons have energy that surpasses the obstructive force as illustrated in Figure S2a.

In contrast, a tunnel diode in which electrons can pass through a narrow barrier is depicted in Figure S2b. The device itself can operate in two modes: (i) tunneling mode and (ii) typical p-n junction mode as shown in Figure S3. It can be explained as follows. At a stage where bias voltage drops to zero (Figure S3a), the conduction band of the n-type sits below the valence band of the p-type. By applying small bias (Figure S3b), electrons can tunnel through the depletion region, resulting in the current flow from the conduction band of the n-side to the valence band of the p-side. In this scenario, the rise of the bias voltage increases the probability of electrons flowing, corresponding to the tunneling effect, until the conduction band of the n-side and the valence band of the p-side become fully overlapped (Figure S3c). As a result, there is a peak current (I_p) at a specific bias voltage (V_p). Increasing the voltage level causes these bands to begin to separate (Figure S3d), and the chance of electron tunneling declines until the

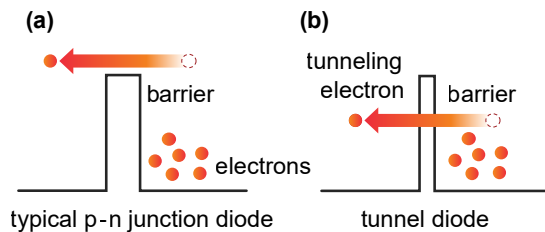


FIG. S2. Current flow (a) in a typical p-n junction diode where only electrons having energy greater than the potential barrier can cross the barrier and (b) in a tunnel diode having a very thin barrier through which electrons can tunnel.

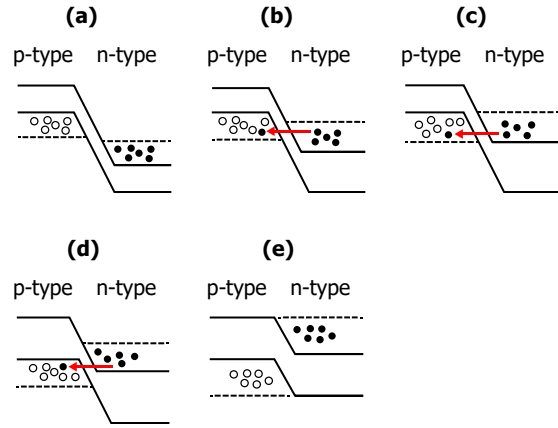


FIG. S3. Energy levels of the tunnel diode at different scenarios: (a) at normal stage without bias voltage, (b) with just enough bias voltage to cause the conduction band of the n-type to overlap with the valence band of the p-type, (c) when the valence band of the n-type fully overlaps with the valence band of the p-type and current flow is maximally dominated from the quantum tunneling effect, (d) when the overlap grows misaligned with a higher bias voltage such that quantum tunneling effect declines, and (e) at the final stage where high voltage drives the tunnel diode to operate in the typical p-n junction diode.

bands are fully out of alignment at a certain voltage (V_v) (Figure S3e). At V_v , the tunneling effect diminishes and therefore provides no contribution to the current flow (I_v). During V_p to V_v , where current and biased voltage translate in the opposite direction, negative resistance behavior is exhibited. Applying more voltage will drive the tunnel diode to operate in a typical p-n junction state where current and biased voltage translate in the same direction.

REFERENCES AND NOTES

- Random numbers are employed for the estimation for the value of pi in the Buffon's needle problem. See <http://www.cut-the-knot.org/fta/Buffon/buffon9.shtml> (Accessed 1 May 2021).
- C. H. Bennett and G. Brassard, "Quantum cryptography: Public key distribution and coin tossing," Proceedings of IEEE International Conference on Computers, Systems and Signal Processing **17**, 8 (1984).
- A. K. Ekert, "Quantum cryptography based on bell's theorem," *Physical Review Letters* **67**, 661–663 (1991).
- P. D. Townsend, "Secure key distribution system based on quantum cryptography," *Electronics Letters* **30**, 809–811 (1994).
- H.-K. Lo, X. Ma, and K. Chen, "Decoy state quantum key distribution," *Physical Review Letters* **94**, 230504 (2005).
- Y. Zhao, B. Qi, and H.-K. Lo, "Experimental quantum key distribution with active phase randomization," *Applied Physics Letters* **90**, 044106 (2007).
- P. Zhang, K. Aungkunsiri, E. Martín-López, J. Wabnig, M. Lobino, R. W. Nock, J. Munns, D. Bonneau, P. Jiang, H. W. Li, A. Laing, J. G. Rarity, A. O. Niskanen, M. G. Thompson, and J. L. O'Brien, "Reference-frame-independent quantum-key-distribution server with a telecom tether for an on-chip client," *Physical Review Letters* **112**, 130501 (2014).
- D. Crnjac Milić and L. Kvesić, "Role of random numbers in simulations of economic processes," *Interdisciplinary management research* **4**, 562–570 (2008).

- ⁹D. Johnston, *Random Number Generators—Principles and Practices: A Guide for Engineers and Programmers* (Walter de Gruyter GmbH & Co KG, 2018).
- ¹⁰P. L'Ecuyer, "Software for uniform random number generation: Distinguishing the good and the bad," in *Proceeding of the 2001 Winter Simulation Conference (Cat. No. 01CH37304)*, Vol. 1 (IEEE, 2001) pp. 95–105.
- ¹¹J. T. Gleeson, "Truly random number generator based on turbulent electroconvection," *Applied Physics Letters* **81**, 1949–1951 (2002).
- ¹²A. Uchida, K. Amano, M. Inoue, K. Hirano, S. Naito, H. Someya, I. Oowada, T. Kurashige, M. Shiki, S. Yoshimori, K. Yoshimura, and P. Davis, "Fast physical random bit generation with chaotic semiconductor lasers," *Nature Photonics* **2**, 728–732 (2008).
- ¹³I. Reidler, Y. Aviad, M. Rosenbluh, and I. Kanter, "Ultrahigh-speed random number generation based on a chaotic semiconductor laser," *Physical Review Letters* **103**, 024102 (2009).
- ¹⁴A. Argyris, S. Deligiannidis, E. Pikasis, A. Bogris, and D. Syvridis, "Implementation of 140 gb/s true random bit generator based on a chaotic photonic integrated circuit," *Optics Express* **18**, 18763–18768 (2010).
- ¹⁵M. J. Wishon, N. Li, D. Choi, D. S. Citrin, and A. Locquet, "Chaotic laser voltage: An electronic entropy source," *Applied Physics Letters* **112**, 261101 (2018).
- ¹⁶K. H. Park, S. M. Park, B. G. Choi, J. B. Kim, and K. J. Son, "High rate true random number generator using beta radiation," *AIP Conference Proceedings* **2295**, 020020 (2020).
- ¹⁷D. G. Marangon, G. Vallone, and P. Villoresi, "Random bits, true and unbiased, from atmospheric turbulence," *Scientific Reports* **4**, 5490 (2014).
- ¹⁸C. S. Petrie and J. A. Connelly, "A noise-based ic random number generator for applications in cryptography," *IEEE Transactions on Circuits and Systems I: Fundamental Theory and Applications* **47**, 615–621 (2000).
- ¹⁹F. Galton, "Dice for statistical experiments," *Nature* **42**, 13–14 (1890).
- ²⁰L. Oberreiter and I. Gerhardt, "Light on a beam splitter: More randomness with single photons," *Laser & Photonics Reviews* **10**, 108–115 (2016).
- ²¹J. G. Rarity, P. C. M. Owens, and P. R. Tapster, "Quantum random-number generation and key sharing," *Journal of Modern Optics* **41**, 2435–2444 (1994).
- ²²A. Stefanov, N. Gisin, O. Guinnard, L. Guinnard, and H. Zbinden, "Optical quantum random number generator," *Journal of Modern Optics* **47**, 595–598 (2000).
- ²³T. Jennewein, U. Achleitner, G. Weihs, H. Weinfurter, and A. Zeilinger, "A fast and compact quantum random number generator," *Review of Scientific Instruments* **71**, 1675–1680 (2000).
- ²⁴Y.-Q. Nie, L. Huang, Y. Liu, F. Payne, J. Zhang, and J.-W. Pan, "The generation of 68 Gbps quantum random number by measuring laser phase fluctuations," *Review of Scientific Instruments* **86**, 063105 (2015).
- ²⁵F. Xu, B. Qi, X. Ma, H. Xu, H. Zheng, and H.-K. Lo, "Ultrafast quantum random number generation based on quantum phase fluctuations," *Optics Express* **20**, 12366–12377 (2012).
- ²⁶Y. Shi, B. Chng, and C. Kurtsiefer, "Random numbers from vacuum fluctuations," *Applied Physics Letters* **109**, 041101 (2016).
- ²⁷T. Symul, S. M. Assad, and P. K. Lam, "Real time demonstration of high bitrate quantum random number generation with coherent laser light," *Applied Physics Letters* **98**, 231103 (2011).
- ²⁸Y.-Q. Nie, H.-F. Zhang, Z. Zhang, J. Wang, X. Ma, J. Zhang, and J.-W. Pan, "Practical and fast quantum random number generation based on photon arrival time relative to external reference," *Applied Physics Letters* **104**, 051110 (2014).
- ²⁹M. Wahl, M. Leifgen, M. Berlin, T. Röhlicke, H.-J. Rahn, and O. Benson, "An ultrafast quantum random number generator with provably bounded output bias based on photon arrival time measurements," *Applied Physics Letters* **98**, 171105 (2011).
- ³⁰R. Bernardo-Gavito, I. E. Bagci, J. Roberts, J. Sexton, B. Astbury, H. Shokeir, T. McGrath, Y. J. Noori, C. S. Woodhead, M. Missous, U. Roedig, and R. J. Young, "Extracting random numbers from quantum tunnelling through a single diode," *Scientific Reports* **7**, 17879 (2017).
- ³¹P. V. Vezeteu, I. I. Popescu, and D. I. Nastac, "The generation of random numbers using the quantum tunnel effect in transistors," in *2019 IEEE 25th International Symposium for Design and Technology in Electronic Packaging (SIITME)* (2019) pp. 379–382.
- ³²A. Fukushima, T. Seki, K. Yakushiji, H. Kubota, H. Imamura, S. Yuasa, and K. Ando, "Spin dice: A scalable truly random number generator based on spintronics," *Applied Physics Express* **7**, 083001 (2014).
- ³³C. Won Ho, L. Yang, K. Jongyeon, A. Deshpande, K. Gyuseong, W. Jian-Ping, and C. H. Kim, "A magnetic tunnel junction based true random number generator with conditional perturb and real-time output probability tracking," in *2014 IEEE International Electron Devices Meeting* (2014) pp. 12.5.1–12.5.4.
- ³⁴D. Vodenicarevic, N. Locatelli, A. Mizrahi, J. S. Friedman, A. F. Vincent, M. Romera, A. Fukushima, K. Yakushiji, H. Kubota, S. Yuasa, S. Tiwari, J. Grollier, and D. Querlioz, "Low-energy truly random number generation with superparamagnetic tunnel junctions for unconventional computing," *Physical Review Applied* **8**, 054045 (2017).
- ³⁵J. Qin, X. Wang, T. Qu, C. Wan, L. Huang, C. Guo, T. Yu, H. Wei, and X. Han, "Thermally activated magnetization back-hopping based true random number generator in nano-ring magnetic tunnel junctions," *Applied Physics Letters* **114**, 112401 (2019).
- ³⁶L. Esaki, "New phenomenon in narrow germanium $p-n$ junctions," *Physical Review* **109**, 603–604 (1958).
- ³⁷K. Aungskunsiri, R. Amarit, K. Wongpanya, S. Saiburee, S. Chanhorm, A. Intarapanich, and S. Sumriddetchkajorn, "Random number generation from a quantum tunnelling diode," [arXiv:2002.02032v1 \[physics.app-ph\]](https://arxiv.org/abs/2002.02032v1) (2020).
- ³⁸Our preliminary work first appeared electronically in [arXiv³⁷](https://arxiv.org/abs/2002.02032v1), and was presented in the LAMP Poster Session held during the Winter College on Optics: Quantum Photonics and Information, ICTP, Trieste - Italy, 10-12 February 2020.
- ³⁹M. S. Turan, E. Barker, J. Kelsey, K. A. McKay, M. L. Baish, and M. Boyle, "Recommendation for the entropy sources used for random bit generation," *NIST Special Publication 800-90B* (2018).
- ⁴⁰See https://github.com/usnistgov/SP800-90B_EntropyAssessment for NIST SP800-90B Entropy Assessment. (Accessed 1 July 2021).
- ⁴¹A. Rukhin, J. Soto, J. Nechvatal, E. Barker, S. Leigh, M. Levenson, D. Banks, A. Heckert, J. Dray, and S. Vo, "A statistical test suite for random and pseudorandom number generators for cryptographic applications," *NIST Special Publication 800-22, Revision 1A* (2010).
- ⁴²X. Ma, F. Xu, H. Xu, X. Tan, B. Qi, and H.-K. Lo, "Postprocessing for quantum random-number generators: Entropy evaluation and randomness extraction," *Physical Review A* **87**, 062327 (2013).
- ⁴³Z. Zheng, Y. Zhang, W. Huang, S. Yu, and H. Guo, "6 Gbps real-time optical quantum random number generator based on vacuum fluctuation," *Review of Scientific Instruments* **90**, 043105 (2019).
- ⁴⁴W. Killmann and W. Schindler, "A proposal for: Functionality classes for random number generators," *ser. BDI, Bonn* (2011).
- ⁴⁵J. Balasch, F. Bernard, V. Fischer, M. Grujić, M. Laban, O. Petura, V. Rožić, G. v. Battum, I. Verbauwhede, M. Wakker, and B. Yang, "Design and testing methodologies for true random number generators towards industry certification," in *2018 IEEE 23rd European Test Symposium (ETS)* (2018) pp. 1–10.